A FEASIBLE MEMRISTIVE CHUA'S CIRCUIT VIA BRIDGING A GENERALIZED MEMRISTOR*

Quan Xu[1], Ning Wang[1], Bocheng Bao[1,†], Mo Chen[1]
and Changdi Li[1]

Abstract By bridging a generalized memristor between a passive LC oscillator and an active RC filter, a simple and feasible memristive Chua's circuit is presented. The generalized memristor without grounded limitation is equivalently achieved by a full-wave rectifier cascaded with a first-order parallel RC filter. The dynamical characteristics of the proposed circuit are investigated both theoretically and numerically, from which it can be found that the circuit has three unstable equilibrium points and demonstrates complex nonlinear phenomena. The experimental circuit is easy to implement and the measurement results validate the results of theoretical analyses.

Keywords Generalized memristor, bifurcation, attractor, chaotic circuit.

MSC(2010) 34A15, 34A23, 34A45, 74H65.

1. Introduction

Memristor, characterized by nonlinear constitutive relation of charge and flux [9], was first hypothesized to be the fourth fundamental circuit element and was achieved physically by TiO_2 nano-scale materials in 2008 [18]. Due to the unique memory characteristics of memristors, the memristor-based circuits are expected to play an important role in many applications [8,12,13,15,19,20], which immensely inspire research interests in the designs of various memristive application circuits. Because of natural nonlinearity of memristor, memristor-based circuit is a nonlinear dynamical circuit and can easily generate chaotic signal with complex dynamical behaviors. Thus, memristor-based chaotic circuit is one of the most important memristive application circuits and receives much attention in recent years. Unfortunately, due to technical handicaps in fabricating nano-scale devices, various kinds of memristive equivalent circuits which can manifest the three fingerprints of memristors [1] have attracted much attention [5]. Indeed, Kim et al. have presented a memristor emulator which provides an alternative solution of Hp TiO_2 memristor model [16]. On the other hand, several nonlinearities for emulating active flux-controlled memristors have been built, such as smooth piecewise-quadratic nonlinearity, smooth cubic nonlinearity, and so on [4, 5, 17]. They are pedagogically useful and serial expandable, but difficult in connecting with other circuit elements in series, which reduces and limits the spread-ability of their work. Fortunately, Corinto et al. [10]

---

have proposed a generalized memristor without grounded restrictions which is realized by a full-wave rectifier cascaded with a second-order LCR filter. Based on this, Bao et al. proposed a simplified generalized memristor by substituting the second-order LCR filter with a first-order parallel RC filter, which leads to that the mathematical model is simple and feasible for numerical simulations [6].

Recently, by introducing memristors characterized by different nonlinearities into various kinds of Chua's chaotic circuits, including Chua's circuit [7], canonical Chua's circuit [14], and modified Chua's circuit [2], a wide class of memristive Chua's chaotic circuits have been presented and investigated broadly. In this paper, we propose a new memristive Chua's circuit, which is realized by bridging the simplified generalized memristor between a passive LC oscillator and an active RC filter. Unlike the other memristive Chua's chaotic circuits in Refs. [11, 16, 17], the introduced generalized memristor works as a general nonlinear element and can be linked into any application circuits in series.

The paper is organized as follows. The general architecture of the proposed memristive Chua's circuit and its dynamical modeling are presented in section 2. The dissipativity and stabilities at the equilibrium points for the circuit are described in section 3. The complex dynamical behaviors are elaborated by bifurcation diagrams, Lyapunov exponent spectra and typical chaotic attractors in section 4. The experimental measurements for specific choices of circuit parameters are shown in section 5. The main conclusions of our work are summarized in section 6.

2. Feasible memristive Chua's circuit

Based on the topology of Chua's circuit, a simple and feasible memristive Chua's circuit is easily constructed, as shown in Figure 1(a), in which the generalized memristor stands for the equivalent realization circuit shown in Figure 1(b) [6]. The mathematical descriptions for the applied voltage v, the generated current i, and the state voltage v_0 are formulated as

$$i = G_M v = 2I_S e^{-\rho v_0} \sinh(\rho v), \qquad (2.1)$$

$$\frac{\mathrm{d}v_0}{\mathrm{d}t} = \frac{2I_S(e^{-\rho v_0}\cosh(\rho v) - 1)}{C_0} - \frac{v_0}{R_0 C_0}, \qquad (2.2)$$

where, $\rho = 1/(2nV_T)$, I_S, n, and V_T represent the reverse saturation current, emission coefficient, and thermal voltage of the diode, respectively. When four 1N4148 diodes are utilized in Figure 1(b), the diode parameters are determined by $I_S = 6.89$ nA, $n = 1.83$, and $V_T = 26$ mV. Thus, the proposed memristive Chua's circuit is equivalent to a fourth-order nonlinear circuit and has four dynamic elements of the capacitor C_1, the capacitor C_2, the inductor L and the capacitor C_0, corresponding to four state variables of v_1, v_2, i_L and v_0. Applying Kirchhoff's laws and the constitutive relations of the circuit elements, a state equation set can be written as

$$\frac{\mathrm{d}v_1}{\mathrm{d}t} = \frac{2I_S e^{-\rho v_0}\sinh[\rho(v_2 - v_1)]}{C_1} + \frac{Gv_1}{C_1},$$

$$\frac{\mathrm{d}v_2}{\mathrm{d}t} = \frac{-i_L - 2I_S e^{-\rho v_0}\sinh[\rho(v_2 - v_1)]}{C_2},$$

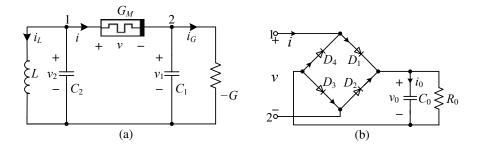$$\frac{\mathrm{d}i_L}{\mathrm{d}t} = \frac{v_2}{L},$$

Figure 1. Memristive Chua's circuit via bridging a generalized memristor. (a) memristive Chua's circuit, (b) realization of generalized memristor.
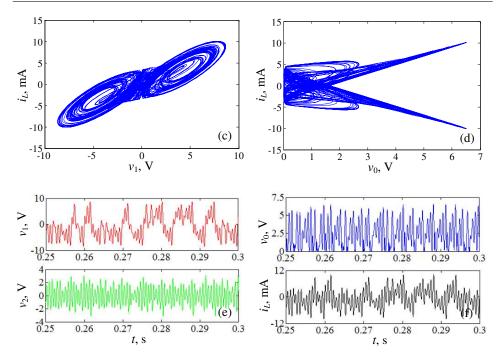
$$\frac{\mathrm{d}v_0}{\mathrm{d}t} = \frac{2I_S e^{-\rho v_0}\cosh[\rho(v_2 - v_1)] - 2I_S}{C_0} - \frac{v_0}{R_0 C_0}, \qquad (2.3)$$

where negative resistor $G = 1/R$ is connected in parallel to the capacitor C_1.

The typical parameters of the circuit in Figure 1 are given in Table 1, and the initial values of four state variables are fixed at (0.1 mV, 0 V, 0 A, 0 V). In order to investigate the dynamics of the memristive Chua's circuit, we solve equation (2.3) by Runge-Kutta algorithm. The proposed circuit is chaotic and can generate a double-scroll chaotic attractor, as shown in Figure 2.

Table 1. Typical parameters of circuit elements

Parameters	significations	Values
R	Resistance	1.4 kΩ
L	Inductance	45 mH
C_1	Capacitance	40 nF
C_2	Capacitance	150 nF
R_0	Resistance	1 kΩ
C_0	Capacitance	20 nF

Figure 2. Projections of chaotic attractor and corresponding time-domain waveforms. (a) projection on the $v_1 - v_2$ plane, (b) projection on the $v_1 - v_0$ plane, (c) projection on the $v_1 - i_L$ plane, (d) projection on the $v_0 - i_L$ plane, (e) waveforms of $v_1(t)$ and $v_2(t)$, (f) waveforms of $v_0(t)$ and $i_L(t)$.

3. Dissipativity and stability analysis

3.1. Dissipativity

The proposed memristive Chua's circuit shown in Figure 1(a) is dissipative in some parameter regions. The dissipativity can be derived from

$$\nabla V = \frac{\partial \dot{v_1}}{\partial v_1} + \frac{\partial \dot{v_2}}{\partial v_2} + \frac{\partial \dot{i_L}}{\partial i_L} + \frac{\partial \dot{v_0}}{\partial v_0}$$
$$= -2\rho I_S e^{-\rho v_0} \cosh[\rho(v_2 - v_1)](\frac{1}{C_1} + \frac{1}{C_2} + \frac{1}{C_0}) + \frac{G}{C_1} - \frac{1}{R_0 C_0}. \tag{3.1}$$

Considering that the hyperbolic cosine and the exponential function are positive, equation (3.1) can be simplified as

$$\nabla V < \frac{G}{C_1} - \frac{1}{R_0 C_0}. \tag{3.2}$$

For the typical parameters listed in Table 1, we find that equation (3.2) is negative, implying that all trajectories of the system are ultimately confined to a specific sub-set with zero volume, and the asymptotic motion will settle onto an attractor.

3.2. Equilibrium points and its stabilities

The equilibrium points of equation (2.3) are obtained by solving the following e-quations

$$2I_S e^{-\rho v_0} \sinh[\rho(v_2 - v_1)] + Gv_1 = 0, \tag{3.3a}$$

$$i_L + 2I_S e^{-\rho v_0} \sinh[\rho(v_2 - v_1)] = 0, \tag{3.3b}$$

$$v_2 = 0, \tag{3.3c}$$

$$2R_0 I_S e^{-\rho v_0} \cosh[\rho(v_2 - v_1)] - 2R_0 I_S - v_0 = 0. \tag{3.3d}$$

Considering equations (3.3c) and (3.3d), obtain

$$v_1 = \pm\frac{1}{\rho} \operatorname{arcosh}[(\frac{v_0}{2R_0 I_S} + 1)e^{\rho v_0}]. \tag{3.4}$$

Hence, v_1 with opposite sign is a double-valued function of v_0. For simplicity, substituting (3.3c) into (3.3a) and let

$$v_1 = f_1(v_0) = \pm\frac{1}{\rho} \operatorname{arcosh}[(\frac{v_0}{2R_0 I_S} + 1)e^{\rho v_0}], \tag{3.5a}$$

$$v_1 = f_2(v_0) = \pm\frac{2I_S e^{-\rho v_0}}{G} \sinh\left\{\operatorname{arcosh}[(\frac{v_0}{2R_0 I_S} + 1)e^{\rho v_0}]\right\}. \tag{3.5b}$$

The intersection points of $f_1(v_0)$ and $f_2(v_0)$ curves give the solver of $f_1(v_0) = f_2(v_0)$. The values of v_0 represent the locations of the equilibrium points on the v_0-axis and can be obtained through graphic analytic method, as shown in Figure 3. Thus, three equilibrium points are calculated as

$$S_0 = (0, 0, 0, 0),$$
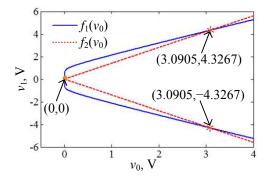$$S_\pm = (\pm 4.3267, 0, \pm 0.0031, 3.0905). \tag{3.6}$$

Figure 3. Two function curves and their intersection points.

The Jacobian matrix of Equation (2.3), evaluated at the equilibrium point $\bar{S} =$

$(\bar{v}_1, \bar{v}_2, \bar{i}_L, \bar{v}_0)$, is given by

$$
\mathbf{J} = \begin{bmatrix}
\frac{G-a_2}{C_1} & \frac{a_2}{C_1} & 0 & -\frac{a_1}{C_1} \\
\frac{a_2}{c2} & -\frac{a_2}{C_2} - \frac{1}{C_2} & \frac{a_1}{C2} \\
0 & \frac{1}{L} & 0 & 0 \\
-\frac{a_1}{C_0} & \frac{a_1}{C_0} & 0 & -\frac{1}{R_0 C_0} - \frac{a_2}{C_0}
\end{bmatrix},
$$

where

$$a_1 = 2\rho I_S e^{-\rho \bar{v}_0} \sinh[\rho(\bar{v}_2 - \bar{v}_1)], \tag{3.7a}$$

$$a_2 = 2\rho I_S e^{-\rho \bar{v}_0} \cosh[\rho(\bar{v}_2 - \bar{v}_1)]. \tag{3.7b}$$

And the corresponding characteristic equation is expressed as

$$\det(\mathbf{1}\lambda - \mathbf{J}) = 0. \tag{3.8}$$

Thus, the four roots at each equilibrium points are calculated as

$$S_0 : \lambda_1 = 17853.52, \lambda_{2,3} = -0.4837 \pm j12171.61, \lambda_4 = -50007.25,$$
$$S_{\pm} : \lambda_{1,2} = 657.59 \pm j8610.31, \lambda_3 = -7944.07, \lambda_4 = -2681630.72. \tag{3.9}$$

Obviously, there are one positive real root, two complex conjugate roots with negative real part and one negative real root at S_0, indicating that S_0 is an unstable saddle point with index 1. It is clearly that the summation of the four roots is negative. Respectively, there are two complex conjugate roots with positive real part and two negative roots at $S_{\pm}$, implying that the pair of non-zero equilibrium points are two unstable saddle-foci with index 2 and the summation of the four roots is negative. The negative summation indicates that the circuit is dissipative. Therefore, a double-scroll chaotic attractor can be emerged at the neighborhoods of two non-zero equilibrium points.

4. Dynamical behaviors

The memristive Chua's circuit has three confirmable equilibrium points. The stability of the circuit is determined by the circuit parameters only. Reversely, for the conventional memristor based chaotic circuits [5], the dynamical behaviors not only depend on the circuit parameters, but also rely on the initial values of the state variables aggressively.

4.1. R_0 as a bifurcation parameter

Firstly, when the inner parameter R_0 of the generalized memristor acts as a varying parameter, the bifurcation diagram of the state variable v_1 and the corresponding Lyapunov exponent spectra of the memristive Chua's circuit are depicted in Figure 4(a) and 4(b), respectively. The bifurcation diagram colored in red (located below) denotes that the orbits starts from the initial values of (-0.1 mV, 0 V, 0 A, 0 V),whereas the other colored in blue (located up) represents that the orbit starts from the initial values of (0.1 mV, 0 V, 0 A, 0 V). Dynamical behaviors with

the coexisting bifurcation modes are observed when $1.062 \text{ k}\Omega \leq R_0 \leq 1.1 \text{ k}\Omega$. For clarity, only first three Lyapunov exponents are presented. In the specific parameter range, the dynamics of the proposed circuit starts from the multi-periodic behaviors and then enters into the chaotic behaviors via a forward period-doubling bifurcation route. In the chaotic region, lots of periodic windows with different periodicities exist, in which the maximum Lyapunov exponent equals to zero.
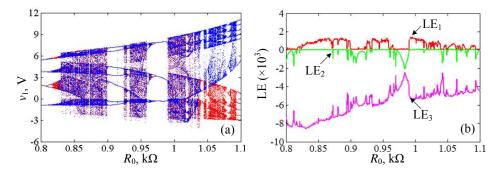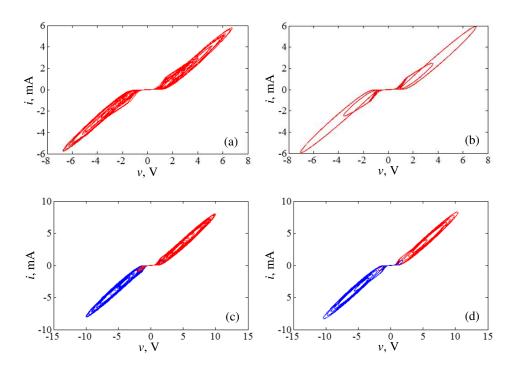

Figure 4. Dynamics respect to R_0. (a) bifurcation diagram of v_1, (b) Lyapunov exponent spectrum.

Figure 5. Chaotic attractors and limit cycles in the $v - i$ plane. (a) chaotic attractor ($R_0 = 0.95$ kΩ), (b) limit cycle with period-3 ($R_0 = 0.98$ kΩ), (c) coexisting spiral chaotic attractors ($R_0 = 1.09$ kΩ), (d) coexisting limit cycles ($R_0 = 1.1$ kΩ).

By numerical simulations, some typical chaotic and periodic orbits of the memristive Chua's circuit are given in Figure 5. Figure 5(a) displays a typical double-scroll chaotic attractor in chaotic region at $R_0 = 0.95$ kΩ. Figure 5(b) illustrates

a typical limit cycle in a periodic window at $R_0 = 0.98$ kΩ. Figure 5(c) and 5(d) demonstrate two coexisting spiral chaotic attractors at $R_0 = 1.09$ kΩ and two coexisting limit cycles at $R_0 = 1.1$ kΩ, respectively. Summarily, with the inner parameter R_0 of the generalized memristor acting as the varying control parameter, complex dynamical behaviors with the coexisting bifurcation modes and the coexisting attractors can be found in the memristive Chua's circuit.

4.2. R as a bifurcation parameter

Also, for the circuit element parameters listed in Table 1, the resistance $R = 1/G$ is regarded as a bifurcation parameter and varies from 1.35 kΩ to 2.35 kΩ. The bifurcation diagram of the state variable v_1 and the corresponding Lyapunov exponent spectrum are depicted in Figure 6(a) and 6(b). The denotations and the initial values are the same as those in Figure 4. The bifurcation diagram well coincides with the Lyapunov exponents spectrum.

When R increases gradually, the dynamics of the circuit begins with the chaotic behaviors and finally settles down the periodic behaviors via reverse a period-doubling bifurcation route. Correspondingly, the maximum Lyapunov exponent has a transition from the positive values to the zero values. There are several periodic windows in which the maximum Lyapunov exponent equals to zero. Dynamical behaviors with the coexisting bifurcation modes are observed when 1.676 kΩ $\leq R_0 \leq 2.35$ kΩ. Observed from Fig. 6, it can be seen that the memristive chaotic circuit exhibits complex dynamical behaviors, including limit cycles, coexisting chaotic spiral attractors, double-scroll chaotic attractor, periodic windows, period doubling bifurcation, chaos crisis and coexisting bifurcation modes.
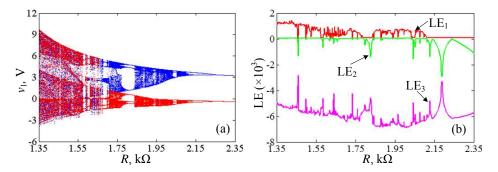

Figure 6. Dynamics respect to R. (a) bifurcation diagram of v_1, (b) Lyapunov exponent spectrum.

Several typical chaotic and periodic orbits of the circuit are obtained, as shown in Figure 7. Figure 7(a) displays a typical double-scroll chaotic attractor in chaotic region at $R = 1.5$ kΩ. Figure 7(b) illustrates two coexisting spiral attractors at $R = 1.95$ kΩ. Figure 7(c) and 7(d) demonstrate two coexisting limit cycles with period-2 at $R = 2.17$ kΩ and two coexisting limit cycles with period-1 at $R = 2.3$ kΩ,respectively. In Figure 7(b), 7(c) and 7(d), the left parts colored in red and the right parts colored in blue stand for that the orbits start from the initial values of (-0.1 mV, 0 V, 0 A, 0 V) and (0.1 mV, 0 V, 0 A, 0 V), respectively. Similarly, with the parameter R acting as the varying parameter, complex dynamical behaviors with the coexisting bifurcation modes and the coexisting attractors can be found.
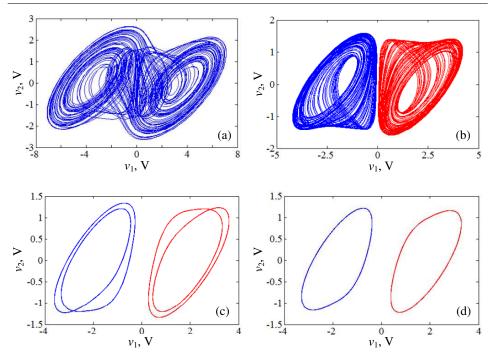
Figure 7. Chaotic attractor and limit cycles in the $v_1 - v_2$ plane. (a) chaotic attractor ($R = 1.5$ kΩ), (b) coexisting spiral attractors ($R = 1.95$ kΩ), (c) coexisting limit cycles with period-2 ($R = 2.17$ kΩ), (d) coexisting limit cycles with period-1 ($R = 2.3$ kΩ).
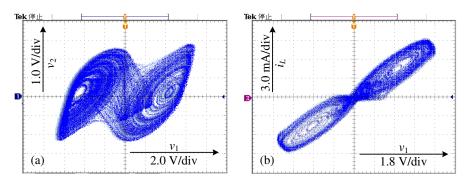
It is noted that for the nonlinear dynamical circuits, their attractors are all emerged from the corresponding unstable equilibria with index-2, i.e., an attractor with a basin of attraction is associated with an unstable equilibrium. Consequently, when the coexisting phenomena occur in the parameter regions of 1.062 kΩ ≤ R_0 ≤ 1.1 kΩ and 1.676 kΩ ≤ R_0 ≤ 2.35 kΩ, two independent basins of attractions are formed, resulting in the generations of coexisting attractors for different initial values.

5. Experimental validations

The experimental observations are presented to validate the complex dynamics of the proposed circuit. An analog electronic circuit can be achieved by commercial available elements. In the experimental circuit, the element parameters are measured as $L = 45.573$ mH, $C_1 = 40$ nF, $C_2 = 150$ nF, and $C_0 = 20$ nF, and OP07CP op-amp is used with a bipolar ±15 V supply.

Experimental results of the phase portraits in the v_1 versus v_2 plane and the v_1 versus i_L plane are shown in Figs. 8(a) and 8(b), respectively, where a double-scroll chaotic attractor can be observed. Both numerical and experimental results are identical.

By keeping $R = 1.4$ kΩ, the chaotic and periodic orbits in the $v - i$ plane are captured in Figure 9 with the variations of the inner parameter R_0 of the generalized memristor. Figure 9(a) illustrates a typical limit cycle with period-3 at

Figure 8. Experimental results of typical chaotic attractor at $R_0 = 1$ kΩ and $R_0 = 1.403$ kΩ. (a) phase portrait in the $v_1 - v_2$ plane, (b) phase portrait in the $v_1 - i_L$ plane.

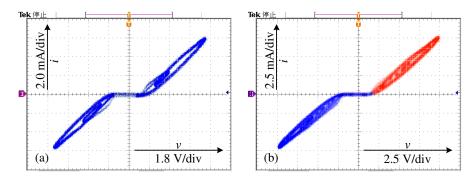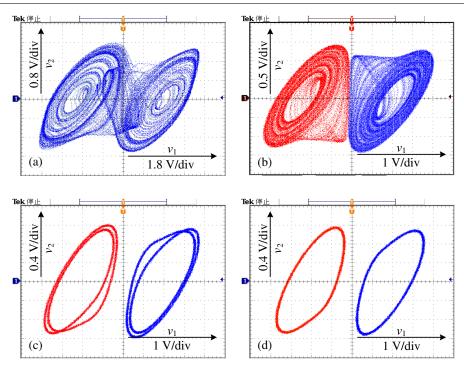**Figure 9.** Chaotic and periodic orbits in the $v - i$ plane. (a) limit cycle with period-3 ($R_0 = 0.986$ kΩ), (b) coexisting spiral chaotic attractors ($R_0 = 1.108$ kΩ).

$R_0 = 0.986$ kΩ. Figure 9(b) demonstrates two coexisting spiral chaotic attractors at $R_0 = 1.108$ kΩ.

As further evidence of complex dynamical behaviors, Figure 10 shows several phase portraits in the $v_1 - v_2$ plane for different values of R experimentally, from which the chaotic attractor, the coexisting chaotic attractors, and the coexisting limit cycles are observed. The reversed initial state is achieved by turning on the circuit power supply again. The experimental observations in different phase planes correspond with the numerical results, and the denotations and the initial values are the same. It indicates that the dynamical behaviors of the experimental analog electronic circuit coincide well versus theoretical analyses of the circuit model.

6. Conclusion

In this paper, a simple and feasible memristive Chua's circuit is presented. The proposed circuit is modeled mathematically by four first-order differential equations. The research results indicate that the circuit has an unstable saddle point with index 1 and a pair of unstable saddle-foci with index 2 in some parameter regions. The dynamical characteristics with the variations of the parameters R_0 and R are investigated. Complex nonlinear phenomena of coexisting bifurcation modes and coexisting attractors are demonstrated in particular. In order to ensure the occurrence of complex nonlinear phenomena, an analog electronic circuit is performed

Figure 10. Chaotic and periodic orbits in the $v_1 - v_2$ plane. (a) double-scroll chaotic attractor ($R = 1.53$ kΩ), (b) coexisting chaotic spiral attractors ($R = 2.05$ kΩ), (c) coexisting limit cycles with period-2 ($R = 2.19$ kΩ), (d) coexisting limit cycles with period-1 ($R = 2.3$ kΩ).

physically, upon which coexisting attractors are captured to validate the correctness and the feasibility of the theoretical analyses.

Acknowledgements

References

[1] S. P. Adhikari, M. P. Sah, H. Kim and L. O. Chua, *Three fingerprints of memristor*, IEEE Trans. Circuits. Syst. I: Reg. Papers., 60(2013)(11), 3008–3021.

[2] B. C. Bao, F. W. Hu, M. Chen and Q. Xu, *Self-excited and hidden attractors found simultaneously in a modified Chuas circuit*, Int. J. Bifurcation and Chaos, 25(2015), 1550075.

[3] B. C. Bao, P. Jiang, H. G. Wu and F. W. Hu, *Complex transient dynamics in periodically forced memristive Chuas circuit*, Nonlinear Dyn., 79(2015), 2333–2343.

[4] B. C. Bao, Z. Liu and J. P. Xu, *Transient chaos in smooth memristor oscillator*, Chin. Phys. B, 19(2010)(3), 158–163.

[5] B. C. Bao, J. P. Xu, G. H. Zhou, Z. H. Ma and L. Zou, *Chaotic memristive circuit: equivalent circuit realization and dynamical analysis*, Chin. Phys. B, 20(2011)(12), 120502–120508.

[6] B. C. Bao, J. J. Yu and F. W. Hu, *Generalized memristor consisting of diode bridge with first order parallel RC filter*, Int. J. Bifurcation and Chaos, 24(2014)(11), 1450143.

[7] M. Chen, M. Y. Li, Q. Yu, B. C. Bao, Q. Xu and J. Wang, *Dynamics of self-excited attractors and hidden attractors in generalized memristor based Chuas circuit*, Nonlinear Dyn., 81(2015), 215–226.

[8] Z. Q. Chen, H. Tang, Z. L. Wang, Q. Zhang and J. W. Han, *Design and circuit implementation for a novel charge-controlled chaotic memristor system*, J. App. Anal. Comput., 5(2015)(2), 251–261.

[9] L. O. Chua, *The fourth element*, Proc. IEEE, 100(2012)(6), 1920–1927.

[10] F. Corinto, and A. Ascoli, *Memristive diode bridge with LCR filter*, Electron. Lett., 48(2012)(14), 824–825.

[11] F. Corinto, A. Ascoli and M. Gilli, *Nonlinear dynamics of memristor oscillators*, IEEE Trans. Circuits. Syst. I: Reg. Papers., 58(2011)(6), 1323–1336.

[12] F. Corinto, A. Ascoli and M. Gilli, *Analysis of currentCvoltage characteristics for memristive elements in pattern recognition systems*, Int. J. Circ. Theor. App., 40(2012)(12), 1277–1320.

[13] K. Eshraghian, K. R. Cho, O. Kavehei, S. K. Kang, D. Abbott and S. M. S. Kang, *Memristor MOS content addressable memory (MCAM): hybrid architecture for future high performance search engines*, IEEE Trans. VLSI Syst., 19(2011)(8), 1407–1417.

[14] A. L. Fitch, D. S. Yu, H. C. IU. Herberth and V. Sreeram, *Hyperchaos in a memristor-based modified canonical Chuas circuit*, Int. J. Bifurcation and Chaos., 22(2012)(6), 1250133.

[15] Y. Ho, G. M. Huang and P. Li, *Dynamical properties and design analysis for nonvolatile memristor memories*, IEEE Trans. Circuits. Syst. I: Reg. Papers., 58(2011)(4), 724–736.

[16] H. Kim, P. S. Maheshwar, C. J. Yang, C. Seongik and L. O. Chua, *Memristor emulator for memristor circuit applications*, IEEE Trans. Circuits. Syst. I: Reg. Papers., 59(2012)(10), 2422–2431.

[17] B. Muthuswamy, *Implementing memristor based chaotic circuits*, Int. J. Bifurcation and Chaos, 20(2010)(5), 1335–1350.

[18] D. B. Strukov, G. S. Snider, D. R. Stewart and R. S. Williams, *The missing memristor found*, Nature, 453(2008)(7191), 80–83.

[19] M. A. Zidan, H. A. H. Fahmy, M. M. Hussain and K. N. Salama, *Memristor-based memory: the sneak paths problem and solutions*, Microelectron. J., 44(2013)(2), 176–183.

[20] M. A. Zidan, H. Omran, C. Smith, A. Syed, A. G. Radwan and K. N. Salama, *A family of memristor-based reactance-less oscillators*, Int. J. Circuits Theor. App., 42(2014)(11), 1103–1122.